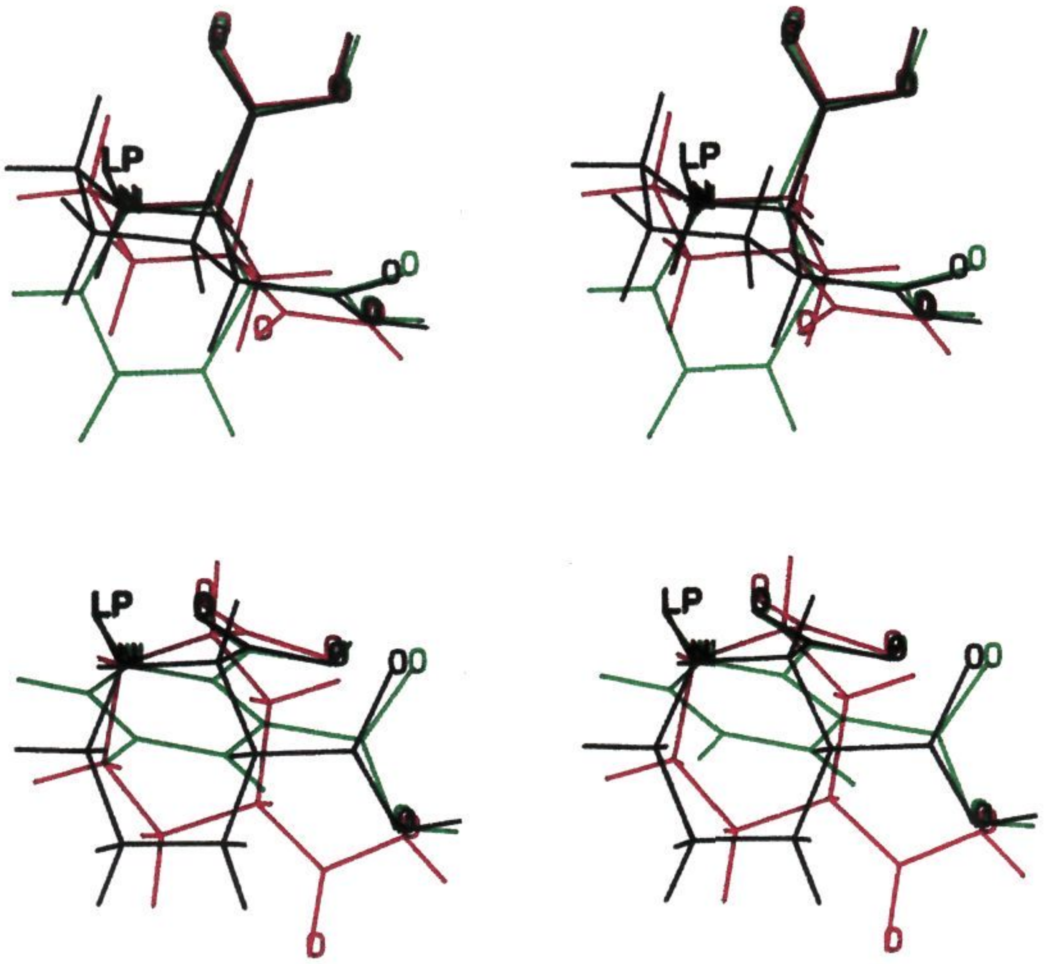

Figure 1. Orthogonal stereoviews of the initial superposition of the basic amine, α-CO_2H, and distal acidic hydroxyl oxygen of the cyclic agonists PDA (**10**, black, and **11**, red) and QUIN (**13**, green). Note the projections of the ketonic oxygen atom of the distal acidic group within **10** and **11** to different areas of space.

and spring energies. When the fit conformations of **7** and **16–18** were relaxed using the MAXIMIN force field, their geometries changed only slightly, reflecting the introduction of significant ring strain and/or out of plane bending of the CO_2H in fitting.[20] Although a MULTIFIT analysis could have been rerun using lower intramolecular spring force constants, the fact that the relaxed structures could still present their pharmacophoric groups in close proximity to their positions as determined by the initial multifit analysis prompted us to do a simple least-squares fit (using the same atoms as were used in the MULTIFIT analysis above) of the relaxed geometries of **16–18** to a reference fit structure (compound **6**) from the initial MULTIFIT analysis. The root mean square (RMS) value for the least-squares fit is shown in Table I beneath the RMS for the MULTIFIT version. No ready explanation is apparent for the relatively high cost of fitting **7** to the consensus multifit cluster. It is possible that its NMDA agonist activity is due in part to interaction with other subsites within the NMDA receptor complex. The relaxed version of **7** was also least-squares fit to the fit version of a reference molecule (**6**); the RMS value for this fit appears below the RMS of the MULTIFIT version.

The proposed agonist pharmacophore model is characterized by a folded conformation in which the planes of the acidic moieties are well defined (Figure 4), thereby positioning these moieties to interact with complementary functionalities at the receptor site. The two acidic groups fall within an average distance separation of 3.5–4 Å (Figure 5), and their planes are inclined 60° relative to each other. They each position an oxygen atom that can engage into a hydrogen-bond interaction with a common receptor site. The tight superposition of the distal acidic hydroxyl but the varying location of the rest of the moiety argues against a charge delocalization between both oxygens of the acid and in favor of a specific hydrogen bond between the acidic hydroxyl and the receptor. A cut-away view of the composite volume occupied by the agonists is shown in Figure 4.

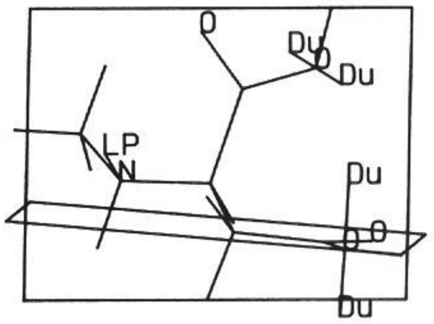

Figure 2. Plot of the fit conformation of NMDA (**6**), showing the planes defined by the acidic groups and the tensors normal to them (Du atoms) piercing through the hydroxyl oxygens. Also shown is the nitrogen lone pair (LP atom) used in the fitting process.

Competitive Antagonist Pharmacophore Model. Although competitive antagonists retain the amino acid portion and distal acidic group that is present in the agonists, the SAR associated with their distal acidic groups differs considerably. In general, potent antagonists contain a distal PO_3H_2 moiety whereas agonists prefer a CO_2H. Although antagonists such as **1** can readily line up their functional moieties on the agonist pharmacophore, they generally occupy additional volume due to their larger structures (Figure 6). Recent reports of relatively rigid, potent antagonists[6b] provided the opportunity to test the assumption of a common binding mode with agonists through the derivation of a separate competitive antagonist pharmacophore model.

---

(20) Another possibility is that MAXIMIN as implemented in version 3.5 of SYBYL was not accurately parameterized to handle cyclic structures such as **16–18**. It was known that small changes in geometry in structures of this type resulted in large calculated energy differences.

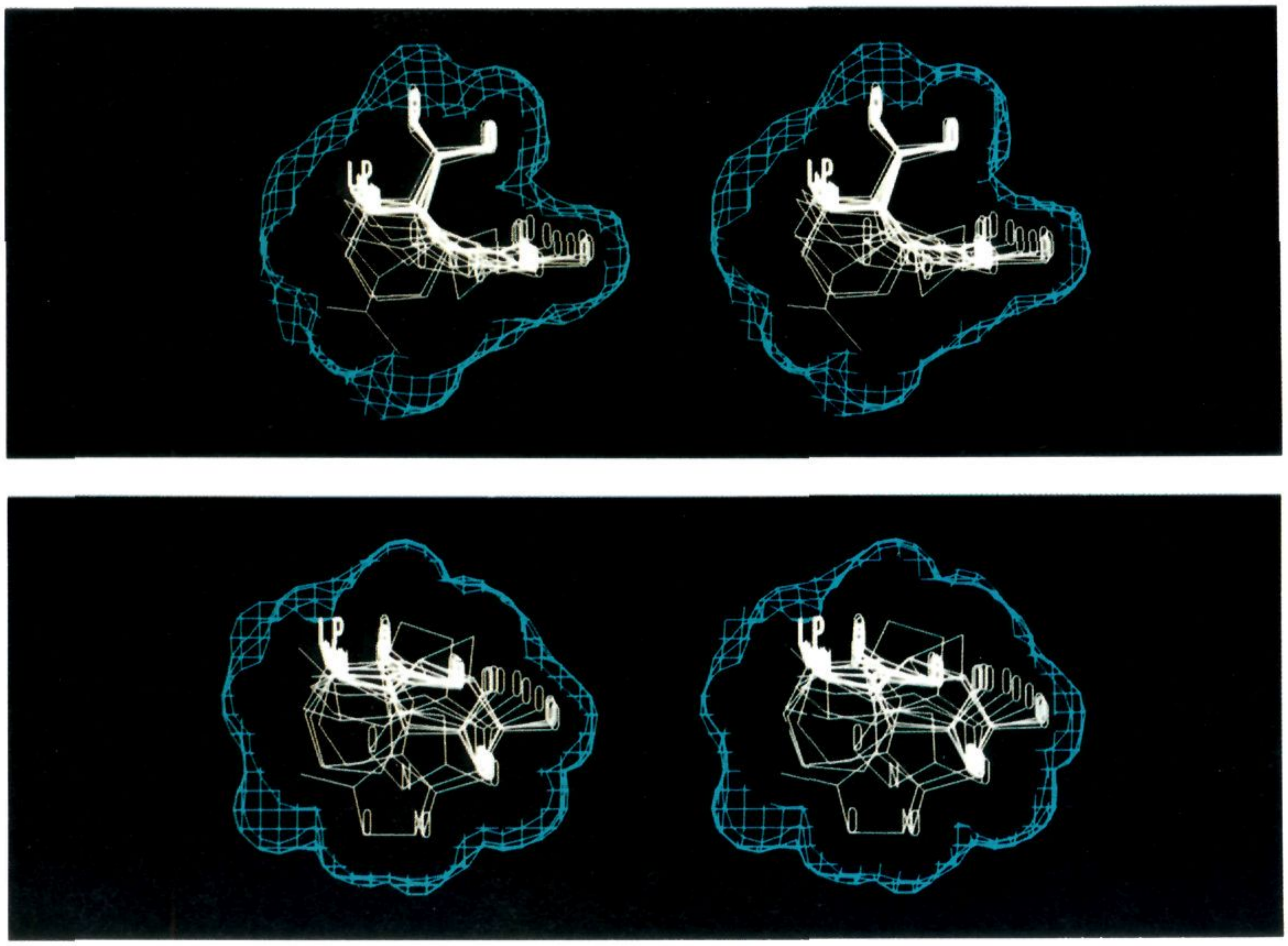

Figure 4. Orthogonal stereoviews of the superposition of the agonists from Figure 2 and Table I. Hydrogens have been removed for clarity. A cut-away view of the composite volume is shown in blue.

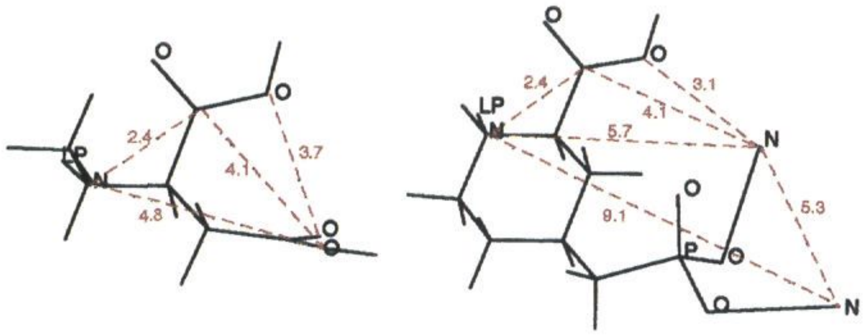

Figure 5. Distances between pharmacophoric groups in the agonist (left) and antagonist (right) models, illustrated using NMDA (**6**) and CGS 19755 (**2**), respectively, in their fit conformations. The nitrogen atoms attached to the PO_3 group represent receptor interactions points (see the antagonist modeling section of the text).

prehensive examinations of the geometry of PO_3H_2–receptor interactions, such as was done with CO_2H[22] groups, have been reported. Therefore, both the Cambridge Structural[23] and Brookhaven Protein[24] databases were searched for $PO_3 \cdots X$ (X = oxygen or nitrogen atoms) noncovalent interactions and the results combined to give average $O \cdots X$ distance and P–O–X valence angle values of 2.8 ± 0.2 Å and 125 ± 15°, respectively (see Tables VII and VIII and the Experimental Section).

Conformational Search Analyses. A hypothetical receptor atom was created that incorporated the PO_3H_2-receptor site point geometry described above. Its energetically allowed positions in space relative to the NH_2 and α-CO_2H were then recorded as conformational searches of the flexible PO_3H_2 side chains of potent antagonists proceeded. By intersecting allowed positions of this receptor atom among potent antagonists, preferred location(s) in common were retained to define an antagonist pharmacophore model.

To accomplish this, the structures of an initial set of antagonists (Table II, top half) were built within SYBYL with extended side chains and rings in chair conformations, and minimized using MAXIMIN[17] (no charges considered), using SYBYL default parameters.[25] Selection was based on available active compounds at the outset of the project, potency, and conformational rigidity. Compounds **22** and

---

(21) Alexander, R. S.; Kanyo, Z. F.; Chirlian, L. E.; Christianson, D. W. Stereochemistry of Phosphate Lewis Acid Interactions: Implications for Nucleic Acid Structure and Recognition. *J. Am. Chem. Soc.* **1990**, *112*, 933–937.

(22) (a) Taylor, R.; Kennard, O. Hydrogen-Bond Geometry in Organic Crystals. *Acc. Chem. Res.* **1984**, *17*, 320–326. (b) Murray-Rust, P.; Glusker, J. P. Directional hydrogen bonding to sp^2- and sp^3-hybridized oxygen atoms and its relevance to ligand-macromolecule interactions. *J. Am. Chem. Soc.* **1984**, *106*, 1018–1025. (c) Vedani, A.; Dunitz, J. D. Lone-Pair Directionality in Hydrogen Bond Potential Functions for Molecular Mechanics Calculations: The Inhibition of Human Carbonic Anhydrase II by Sulfonamides. *J. Am. Chem. Soc.* **1985**, *107*, 7653–7658.

(23) (a) Allen, F. H.; Kennard, O.; Taylor, R. Systematic Analysis of Structural Data as a Research Technique in Organic Chemistry. *Acc. Chem. Res.* **1983**, *16*, 146–153. (b) Allen, F. H.; Bellard, S.; Brice, M. D.; Cartwright, B. A.; Doubleday, A.; Higgs, H.; Hummelink, T.; Hummelink-Peters, B. G.; Kennard, O.; Motherwell, W. D. S.; Rodgers, J. R.; Watson, D. G. The Cambridge Crystallographic Data Centre: Computer-Based Search, Retrieval, Analysis, and Display of Information. *Acta Crystallogr.* **1979**, *B35*, 2331–2339.

(24) (a) Bernstein, F. C.; Koetzle, T. F.; Williams, G. J. B.; Meyer, E. F., Jr.; Brice, M. D.; Rodgers, J. R.; Kennard, O.; Shimanouchi, T.; Tasumi, M. The Protein Data Bank: A Computer-Based Archival File for Macromolecular Structures. *J. Molec. Biol.* **1977**, *112*, 535–542. (b) Abola, E. E.; Bernstein, F. C.; Bryant, S. H.; Koetzle, T. F.; Weng, J. In *Crystallographic Databases-Information Content, Software Systems, Scientific Applications*; Allen, F. H., Bergerhoff, G., Sievers, R., Eds.; Data Commission of the Intern'l. Union of Crystallography: Bonn, 1987; pp 107–132.

Table II (Continued)

no.		IC$_{50}$,^{d} μM	number of distances^{b} unconstrained	constrained^{e}	energies, kcal/mol^{c} fit	relaxed	cost
29^{j}	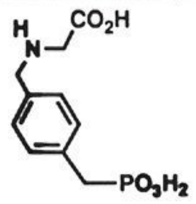	5.2			2.0	0.1	0.6
30^{n}	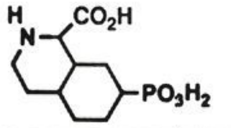	5.6			−6.0	−7.6	0.4

^{a} Structures above the line were used to define the location of the receptor interaction points. Structures below, synthesized during the course of the search analysis, were added to the initial MULTIFIT to more precisely define the locations of the receptor interaction points and to evaluate the energetics of fitting. ^{b} See Figure 8 for an explanation of the distances employed. ^{c} See Table I for an explanation of the energies. Since the RMS deviation between fit atoms was <0.1 Å and the spring energy <1.3 kcal/mol for the compounds in this table, these values were not included. ^{d} For displacement of [^{3}H]CPP from rat brain membranes; see the Experimental Section. ^{e} Searches were constrained to match the set of 378 distances from the search on **2**. ^{f} Not used in the initial MULTIFIT analysis. ^{g} Reference 11. ^{h} Reference 50. ^{i} Reference 51. ^{j} Reference 52. ^{k} References 5, 43. ^{l} Reference 10a. ^{m} Tested as a mixture of stereoisomers; modeled structure was 2*R*,1′*R*,3′*S* isomer. See ref 53. ^{n} Prepared by hydrogenation of **116** with PtO$_2$ at 50 psi and 25 °C, followed by hydrolysis in 6 N HCl at reflux.

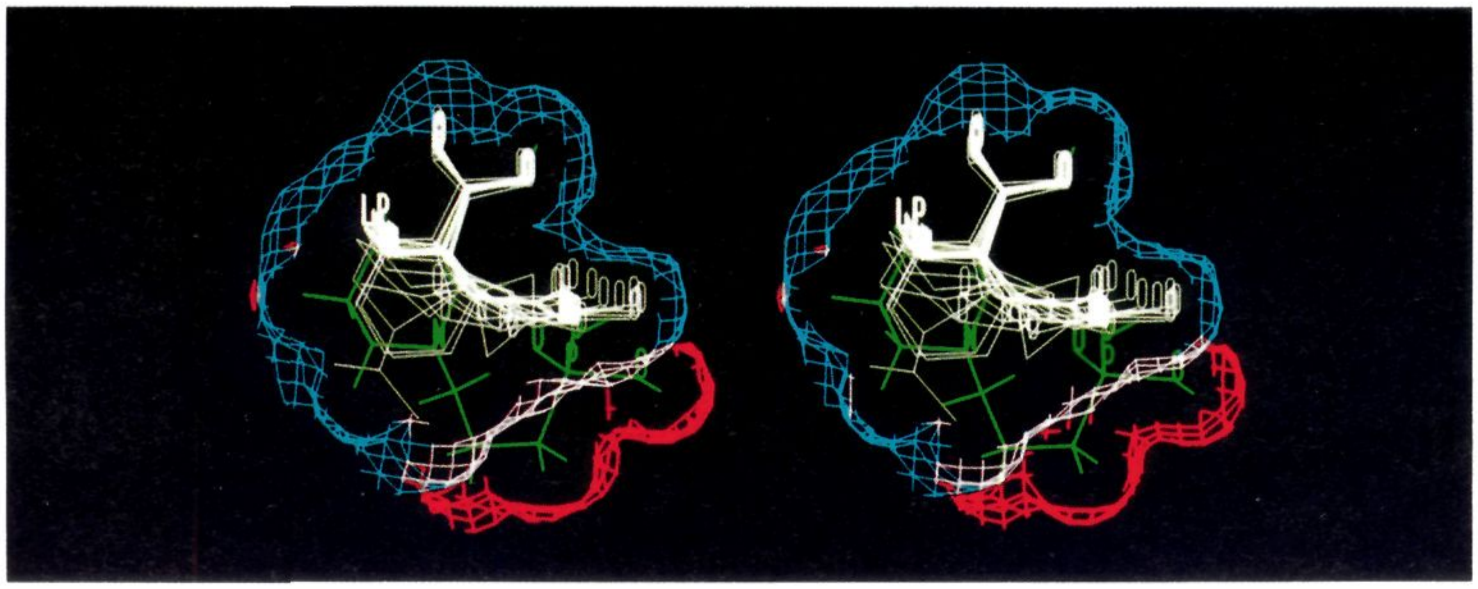

Figure 6. Stereoview of the fit of CPP (1, green) onto the agonist pharmacophore model, in a low energy conformation as determined by a conformational search analysis (see the antagonist modeling section for details). Hydrogens have been removed from the agonists for clarity. In red is shown the volume occupation of the PO$_3$H$_2$ side chain of CPP outside the composite volume of the active agonists.

96, although somewhat less potent, were included since it was felt that their reduced potency was due to factors other than the ability of their distal acidic groups to reach a receptor site point. Specifically, the decreased affinity of **22** could be due to increased entropy and possibly excluded volume, while **96** possessed a phosphonate directly bonded to an aryl ring, a substitution previously found to decrease affinity.[26]

Consistent with literature data on CPP[27] (**1**) and AP5 (**3**),[2] which demonstrated that the *R* stereoisomer at the α-carbon of the amino acid portion was preferred for high affinity, antagonists were built with this atom in the *R* configuration. Because cis-2,4-disubstitution of the cyclohexane ring on antagonists such as **2** was favored over trans (Table III; compare the affinities of **2** and **33**), building the cyclic analogues in the 2*R* configuration resulted in an *S* configuration at the 4-carbon. Therefore, antagonists containing a six-membered saturated rings were constructed as the 2*R*,4*S* isomer.

Charges were then calculated using the CNDO/2[28,29] method. A hypothetical receptor site point (an sp^{3} nitrogen atom) was added to one of the PO$_3$H$_2$ hydroxyl oxygens in the geometry defined by the database searches above, replacing that hydroxyl's hydrogen (Figure 7). A nitrogen atom was chosen because it was felt this would be the smallest heavy atom in a receptor one would normally expect the PO$_3$H$_2$ group to hydrogen bond to. Therefore, in a conformational search setting, use of a van der Walls radius of a nitrogen atom would allow the most conformations to be selected (not rejected due to intermolecular

---

(25) Parameters were unavailable for the C.ar-P.O3 (aromatic carbon to phosphonate phosphorous atom) bond present in several of the antagonists. Stretching, bending, and torsional parameters for a C.2-P.O3 (C.2 = an sp^{2} carbon atom) bond were substituted, and a C.ar-P.O3 equilibrium bond length of 1.76 Å was determined by searching the Cambridge Structural Database[23] for occurrences of C.ar-P.O3 pairs and averaging the resulting bond lengths.

(26) For examples, see refs 10a, 11, and 52b.

(27) Aebischer, B.; Frey, P.; Haerter, H.-P.; Herrling, P. L.; Mueller, W.; Olvermann, H. J.; Watkins, J. C. Synthesis and NMDA Antagonistic Properties of the Enantiomers of 4-(3-Phosphonopropyl)piperazine-2-carboxylic acid (CPP) and of the Unsaturated Analogue (E)-4-(3-Phosphonoprop-2-enyl)-piperazine-2-carboxylic Acid (CPP-ene). *Helv. Chim. Acta* **1989**, *72*, 1043–1051.

(28) (a) Pople, J. A.; Beveridge, D. L. *Approximate Molecular Orbital Theory*, McGraw-Hill: New York, 1970. (b) Structures were passed from SYBYL to CHEMLAB-II[29] (version 10.0) for charge calculations using the CNDO/2 module. Density matrix-derived point charges were used in the calculations. The MOL2 files in the supplementary material contain atomic charges for selected compounds.

(29) (a) Pearlstein, R. A. *CHEMLAB-II Reference Manual*; Chemlab, Inc. (software available from Molecular Design Limited, San Leandro, CA). (b) Childress, T., Ed. Revised MDL Edition, March 1985; Molecular Design Limited, San Leandro, CA.

Table III. Antagonists Used To Define the Receptor-Tolerated Volume[a]

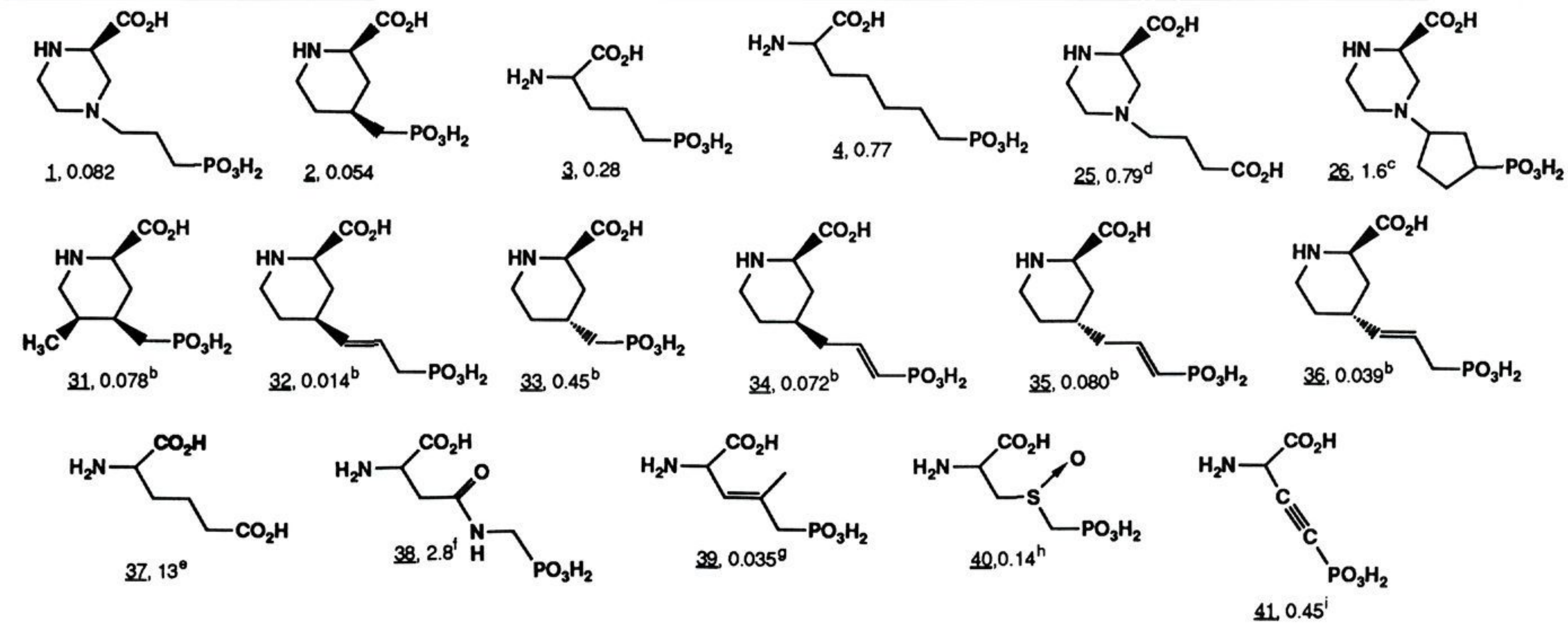

[a] See Figure 13. IC$_{50}$'s (μM) are given after the compound number. A table of fitting energies is included in the supplementary material. [b] Reference 6b. [c] Reference 53b; also see footnote m of Table II. [d] Reference 10a. [e] Reference 2a. [f] References 54, 55. [g] Reference 56. [h] Reference 57. [i] Reference 58.

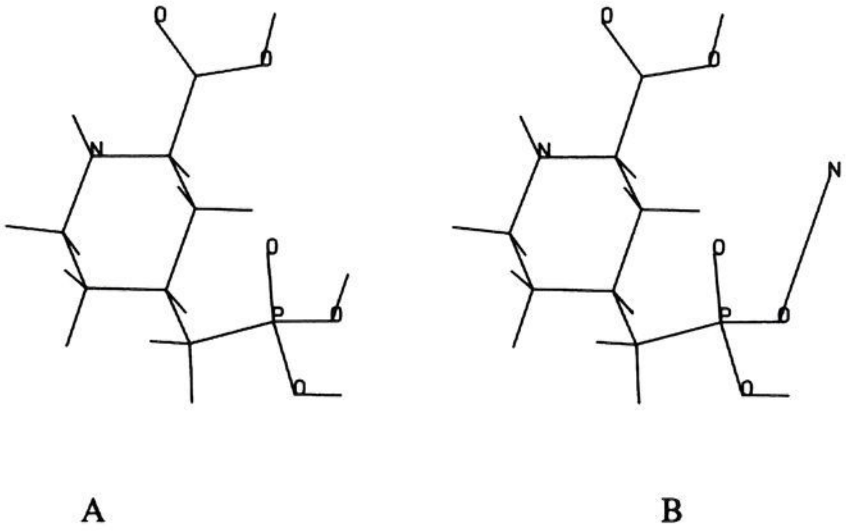

Figure 7. Structure of CGS 19755 (**2**). Version A is the standard molecule as initially constructed and minimized, and version B contains a hypothetical receptor (a nitrogen) atom 2.8 Å from and bonded to one of the PO$_3$ oxygen atoms.

steric contacts). After superimposing the basic amine, its lone pair, and the proximal CO$_2$H, conformational searches were run on the PO$_3$H$_2$ side chains (SYBYL, SEARCH[19] procedure); see the Experimental Section for details. Two methods of recording the position of the receptor site point were investigated. The coordinate map approach (termed vector maps in version 3.5 of SYBYL) failed due to size limitations (the maximum number of vectors that could be recorded [2000] was exceeded in unconstrained searches on molecules such as **1**); the distance map method (termed orientation maps in version 3.5) proved successful in recording allowed receptor atom locations.

By intersecting allowed distances among the active antagonists **1**, **2**, and **19–22** (Table II, Figure 8) and then subtracting distances corresponding to the inactive analogues **23** and **24**, a set of 17 distances resulted that corresponded to 25 conformations of **2** (Figure 9). Intersecting the search results of **96**, a compound that was synthesized after the initial analysis was completed, further constrained the results to a single set of distances (with several near misses) that mapped out a unique area of space for the receptor interaction atom (Figure 10). A representative set of distances from this area was chosen as the location of a receptor interaction, hereafter referred to as the "primary receptor interaction point" (Figure 11).

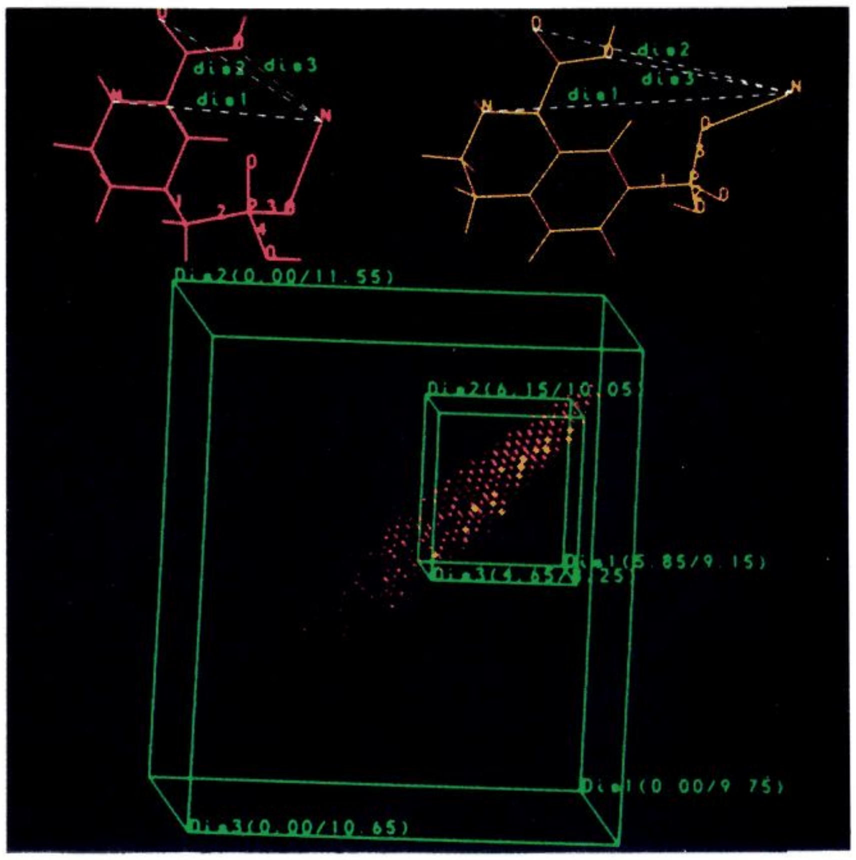

Figure 8. Overlay of distance map recordings for the unconstrained search of CGS 19755 (**2**, red; 378 distances; see Table II) and a constrained search of **96** (yellow; 19 distances). The bonds that were scanned in the search analysis are numbered.

On fitting the active antagonists **1**, **2**, **19–22**, and **96** to this point, a "secondary" receptor interaction point was defined that was capable of a hydrogen-bonding interaction with the other hydroxyl group within the PO$_3$H$_2$ moiety, or a lone pair attached to the ketonic oxygen atom of those antagonists containing a distal CO$_2$H moiety (Figure 12). The third (ketonic) oxygen, while projecting a negative electrostatic potential to the north and northwest portion of the structures as they appear in Figures 9 and 10, did not suggest the formation of a hydrogen bond with a specific receptor atom due to its varying spatial occupation among potent antagonists.

To locate more precisely the primary and secondary receptor interaction points, as well as evaluate the relative energetics of the fit versus relaxed conformations, the fit

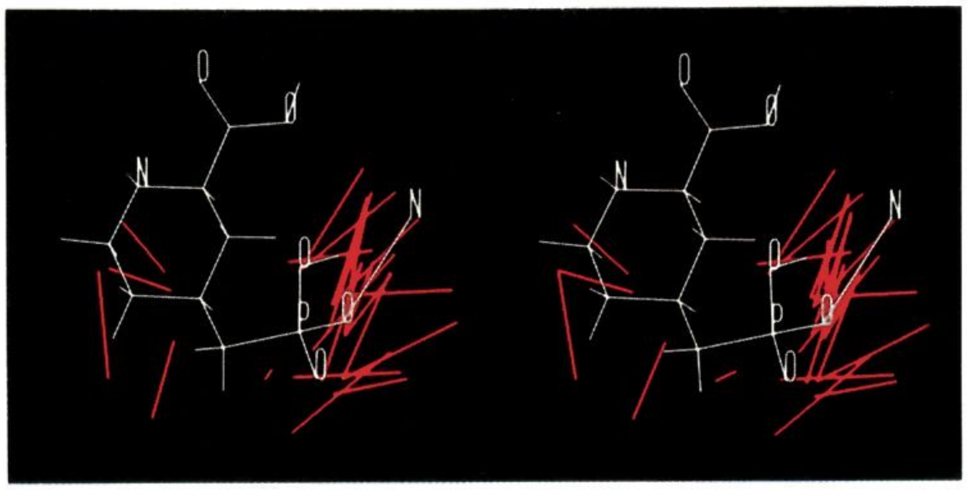

Figure 9. A recording of the P···X (X = an sp^3 nitrogen atom used to represent a receptor interaction) bond (red lines) from the 25 conformations of **2** that could reach the 17 distances resulting from the initial analysis of **1**, **2**, and **19–24** (Table II).

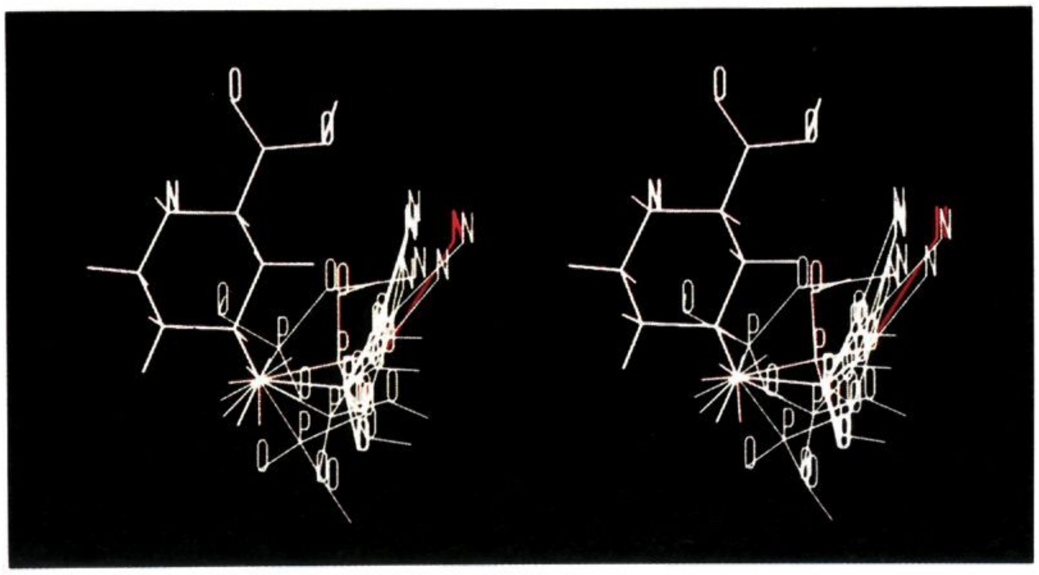

Figure 10. Remaining conformations of **2** after the search results of **96** (both ring conformers) were intersected. The conformer chosen for the initial receptor-site location is shown in red.

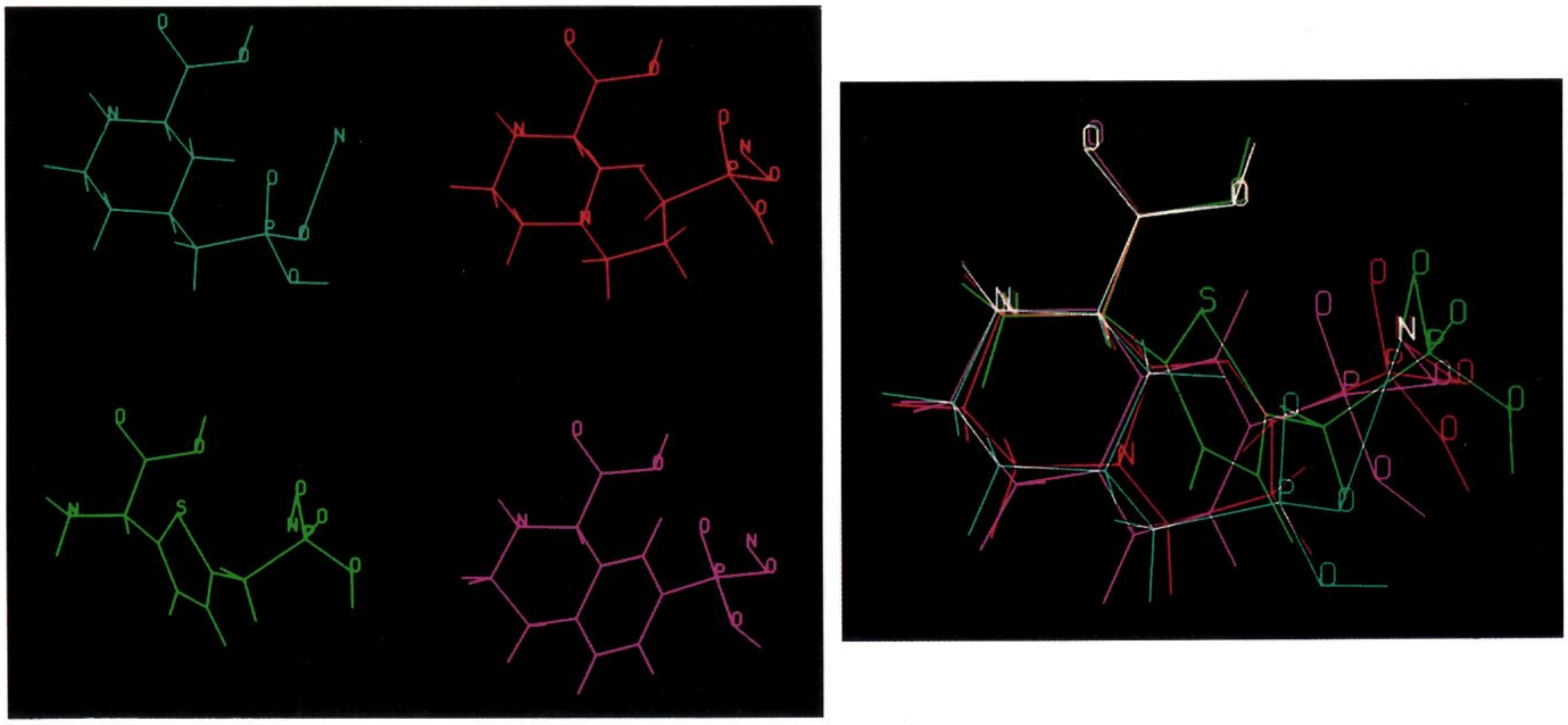

Figure 11. Fit conformations of **1** (red), **2** (aqua), **20** (green), and **96** (purple) (left), and their overlay (right), showing the alignment of the primary receptor interaction point (white N atom).

versions of **1–4**, **19–22**, **96**, and additional active compounds **25–30**, synthesized during the course of the search analyses, were subjected to a MULTIFIT[17] analysis. Similar to the analysis involving the agonists, the structures were built, minimized using MAXIMIN, and oriented with the basic nitrogen at the origin, the α-methylene along the x axis, and the carbon of the proximal CO_2H group in the x–y plane. A 2-Å tensor was defined that was perpendicular to the plane of the proximal CO_2H, piercing through the hydroxyl oxygen. The structures were then constrained to superimpose the endpoints of this tensor, the basic nitrogen, its lone pair, and the receptor interaction points. Intramolecular spring force constants of 20 kcal/mol Å^2 were used on all fitting atoms, except for the secondary receptor interaction point. The spring force constant for this atom was reduced to 10 kcal/mol Å^2 to reflect the somewhat reduced importance of interaction with this site for maintenance of high affinity to the NMDA receptor.[30] Charges were not included in the calculations. After running MULTIFIT, the structures were allowed to relax by rerunning MAXIMIN (without charges) on the multifit geometry without any constraints.

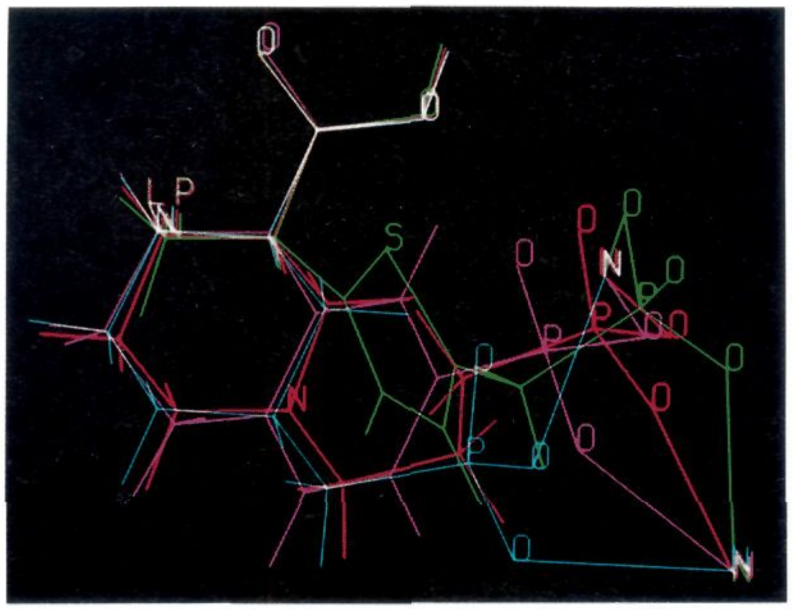

Figure 12. After fitting, it was noted that a secondary interaction point near the other PO_3H_2 hydroxyl group could be defined.

Volume and Electrostatic Computations. Additional antagonists synthesized in our laboratories or reported in the literature subsequent to the initial MULTIFIT analysis were then added to the model by multifitting them to a reference fit compound, **2**, and evaluating the energetics of the fit versus relaxed versions. In this manner, approximately 100 structures were added to the model. Selected compounds that were used in the computation of the receptor-tolerated volume (Figure 13, blue area) appear in Table III. Selection was based on volume contribution—active analogues that did not occupy additional volume outside the composite volume of the structures in Table III were not included.

In general, less potent potent analogues fell into four main categories: (1) those with excluded volume (Tables IV and V); (2) those that lack key structural features such as an α-CO_2H or a primary or secondary basic amine (**85**, Chart I, and **57**, Table V, respectively; compare both with **1**, Table II); (3) those that could not reach one or more of the distal acidic receptor interaction sites (Table II, **23** and **24**); and (4) those with an electrostatic potential pattern different from that exhibited by potent antagonists in key regions (**86**, Chart I; also, **81** and **83**, Table VI; Figure 14). In Table IV are listed compounds used in the computation of volume corresponding to roughly a 10-fold decrease in potency (Figure 15, yellow volume), while structures corresponding to severe receptor excluded volume (>100 fold decrease in potency) appear in Table V (Figures 15 and 16, red volume). Compounds falling into categories 1 and 4 all possessed the key structural features necessary for high affinity and could reach the receptor interaction sites with a minimal energy cost, yet remained markedly less potent.

CNDO/2 charges[28] and electrostatic potentials[31] were calculated for all antagonists fit to the model. Beyond the generally negative (proton attractive) potential associated with the PO_3H_2 and α-CO_2H groups and the neutral to positive potential connected with the lipophilic portions of the structures, a key feature involved the electrostatic potential associated with the third (ketonic) oxygen of the PO_3H_2 group. Although a specific hydrogen bonding receptor interaction point for this atom could not be defined, the presence of this potential and the direction of its projection appeared to be related to antagonist potency. For example, antagonists possessing a distal CO_2H instead of a PO_3H_2 moiety were 10-fold less potent, presumably because they lack this negative potential. Although these analogues could be less potent because they lack volume corresponding to the third oxygen atom of the PO_3H_2, the phosphinic analogue of **1**, which places a methyl group in the same location as the third (ketonic) PO_3H_2 oxygen, is also approximately 10-fold less potent (IC_{50} = 0.78 μM^{10a}).

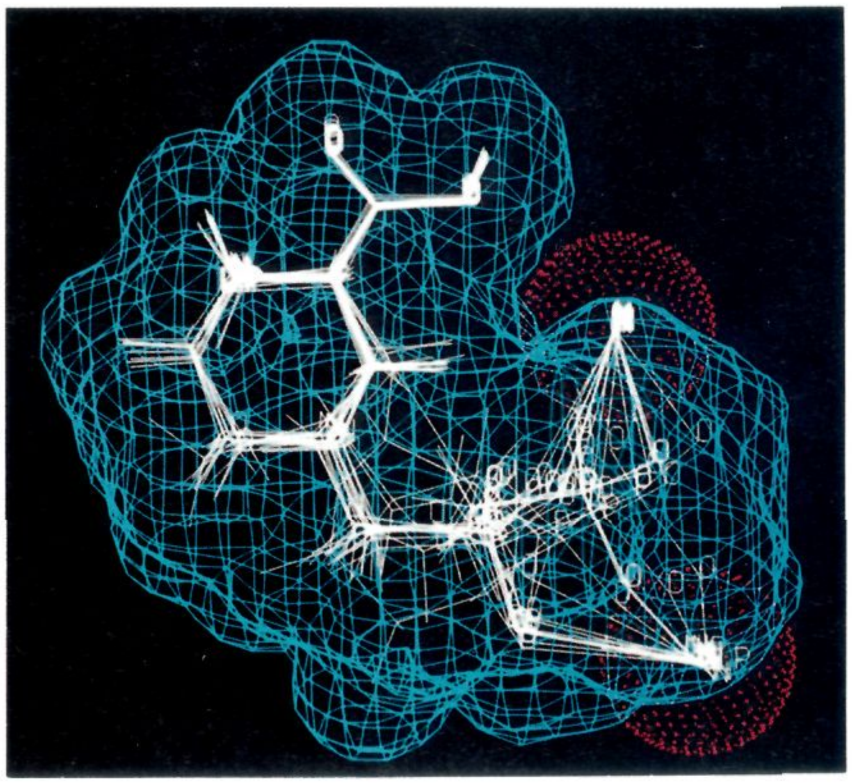

Figure 13. Superposition of 17 potent antagonists (Table III), the composite receptor-tolerated volume (blue), and the receptor-site atoms (white N atoms or lone pair [LP] electrons surrounded by red dots). Lone pairs were used for the receptor-site atoms being interacted with by the ketonic oxygen atom within those antagonists containing distal CO_2H groups (see text).

When AP6 (**81**) and **83** were fit to the model, the ketonic PO_3H_2 oxygen atom projected a negative potential toward the basic amine (Figure 14), which was reflected in part by a larger X component of the dipole moment as calculated via CNDO/2[28] (Table VI, compare μ_x for **3**, **81**, and **4**). This potential may inhibit the approach of a negatively charged receptor atom that must interact with the amine for strong binding. The periodicity in affinity as the PO_3H_2 side chains are lengthened in the AP4-5-6-7 (**80–3–81–4**) and **82–83–1–84** series (Table VI) can be rationalized by this observation.

Results. Similar to the agonist model, the competitive antagonist pharmacophore model entails a folded conformation and contains two specific receptor interaction points off of the distal phosphonic acid (Figures 6 and 17). Both points are roughly in the plane of the piperazine ring of **1**, and one is positioned such that a receptor moiety could simultaneously hydrogen bond to oxygens on the PO_3H_2 and α-CO_2H groups. This point is also in proximity to the distal acidic hydroxyl of the agonist model described above. Similar to other models,[2,6b] strict volume requirements are found near the basic amine, α to the phosphonic acid, and surrounding the receptor interaction sites (Figure 14), presumably reflecting critical receptor interactions occurring in these areas. However, some volume tolerance

---

(30) From the SAR/modeling analyses, there were examples (compounds **37**, **51**, **52**, and **80**) of compounds that, when fit to the "primary" receptor interaction point at the appropriate hydrogen bond length (2.8 Å) and P–O–N valence angle (125°), could not be made to form a strong hydrogen bond with the "secondary" interaction point in a low energy conformation (wrong distance and/or valence angle). These compounds were 10–100x less potent than closely related analogues (**3** and **19**) that could interact with this site at the appropriate geometry. However, compounds (such as **23** and **24**, Table II) not capable of interacting with the "primary" interaction site at the appropriate geometry were markedly less potent (>1000x loss in affinity).

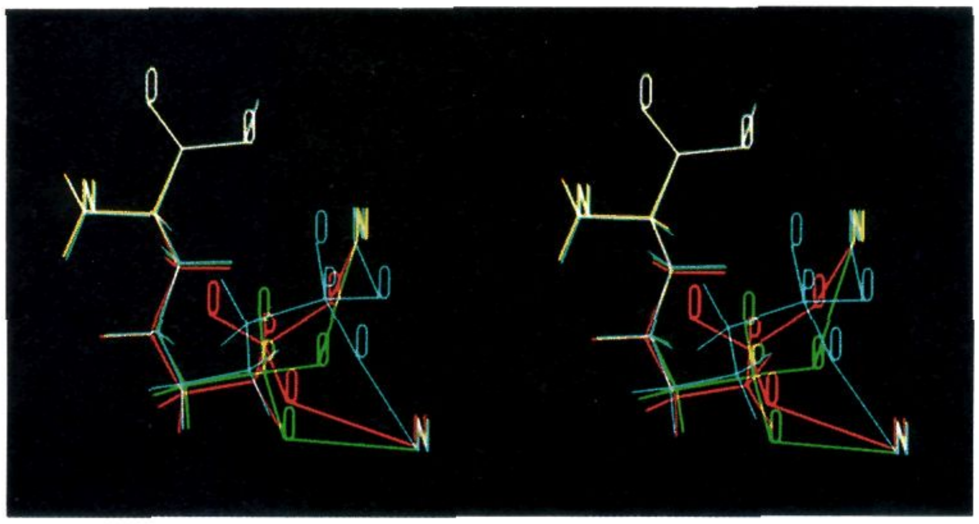

Figure 14. An overlay of the fit versions of **3** (green), **81** (red), and **4** (cyan). Note the direction of projection the ketonic PO_3H_2 oxygen atom (not bonded to the receptor interaction points). The active compounds **3** and **4** project to the north, while the less-potent analogue **81** projects to the northwest, toward the basic NH_2. This is reflected by an increased value calculated for the *x* component of the dipole moment (see text).

Table V. Antagonists Used To Define Severe Receptor-Excluded Volume[a]

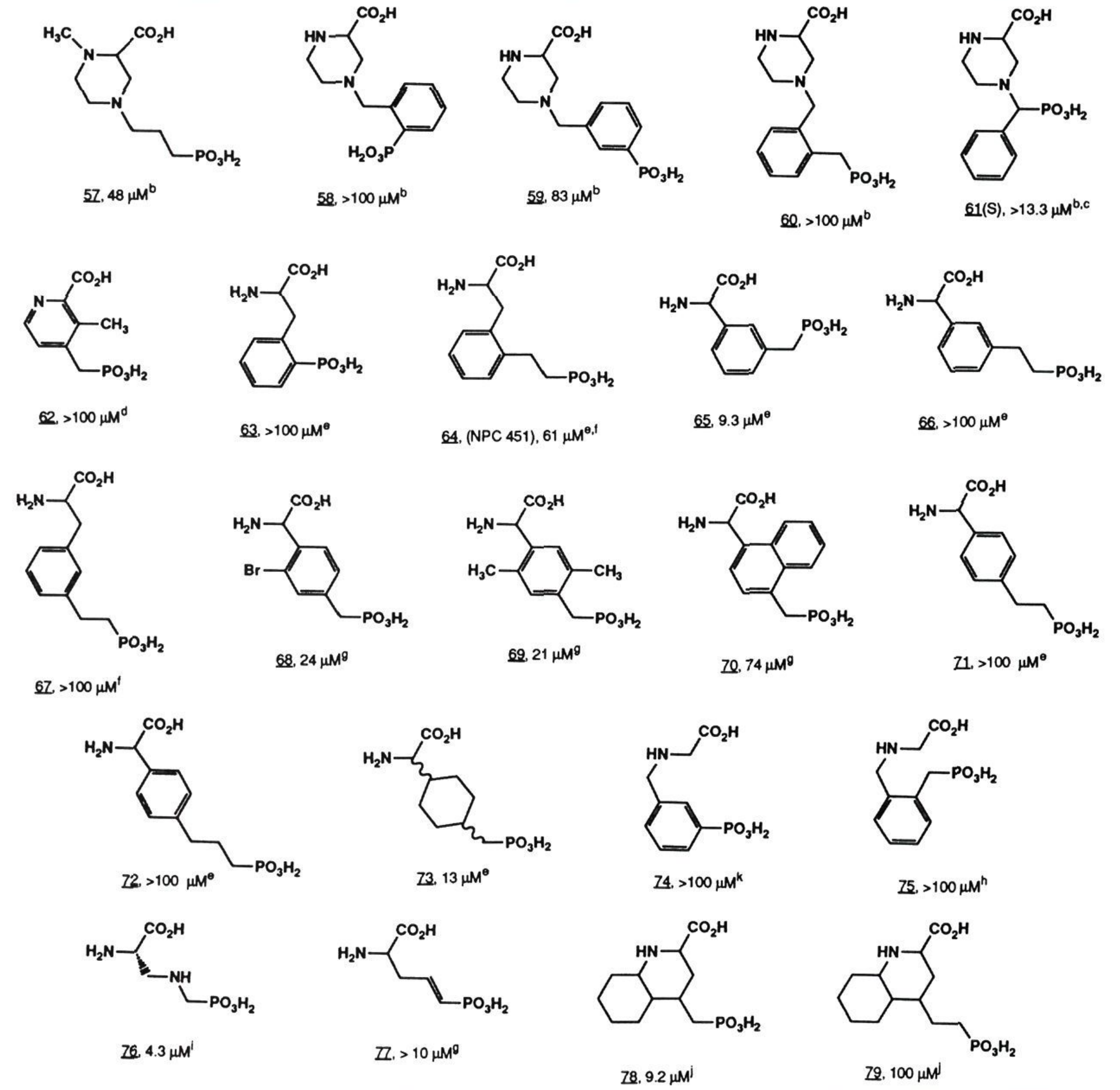

57, 48 μM^{b}

58, >100 μM^{b}

59, 83 μM^{b}

60, >100 μM^{b}

61(S), >13.3 μM^{b,c}

62, >100 μM^{d}

63, >100 μM^{e}

64, (NPC 451), 61 μM^{e,f}

65, 9.3 μM^{e}

66, >100 μM^{e}

67, >100 μM^{f}

68, 24 μM^{g}

69, 21 μM^{g}

70, 74 μM^{g}

71, >100 μM^{e}

72, >100 μM^{e}

73, 13 μM^{e}

74, >100 μM^{k}

75, >100 μM^{h}

76, 4.3 μM^{i}

77, > 10 μM^{g}

78, 9.2 μM^{j}

79, 100 μM^{j}

---

[a] Volume, that if occupied, results in a ≥100-fold decrease in affinity (Figures 15 and 16). IC_{50}'s (μM) are given after the compound number. A table of fitting energies is included in the supplementary material. [b] Reference 10a. [c] Tested as a 1.6:1 mixture of isomers. See **49** in Table IV. [d] Reference 59. [e] Reference 11. [f] Reference 55. [g] Reference 61. [h] Reference 52. [i] Reference 57b. [j] Prepared by hydrogenation of the aromatic ring of the corresponding quinolines with PtO_2 at 50 psi and 25 °C; ref 51.

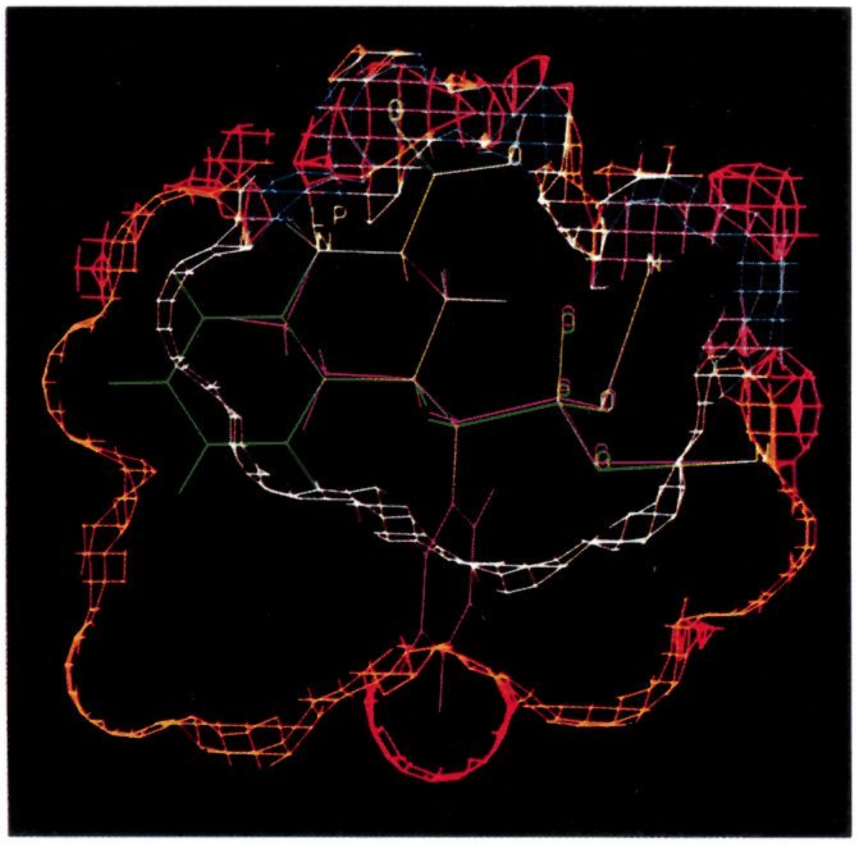

Figure 15. Cut-away view of a portion of the receptor tolerated (blue), moderate (yellow), and severe (red) receptor excluded volumes, with examples of less-potent analogues **21** (green) and **61** (purple) included. The interface between the receptor-tolerated volume and moderate receptor-excluded volume is colored white, and areas where all three volumes intersect is pink.

Table VI. Periodicity in Binding Affinity of Competitive Antagonists

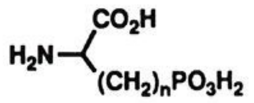

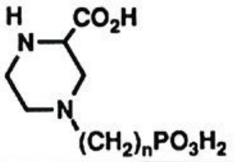

no.	name	n	IC$_{50}$, μM[a]	μ_x[b]	no.	name	n	IC$_{50}$, μM[a]	μ_x[b]
80[c]	AP4	2	>100	3.3					
3	AP5	3	0.28	2.6	**82**[d]		1	0.32	2.0
81[c]	AP6	4	42	5.4	**83**[d]		2	9.8	3.7
4	AP7	5	0.77	1.1	**1**	CPP	3	0.082	0.7
					84[d]		4	48	2.1

[a] For displacement of [^{3}H]CPP from rat brain membranes; see the Experimental Section. [b] X component of the dipole moment, in debyes, calculated from the density matrix via the CNDO/2[28] procedure. [c] Reference 2. [d] Reference 10a.

a previously reported series of aryl APH analogues.[11] Specifically, hybrid derivatives that combined the cyclic amino acid functionality present in known antagonists such as CGS19755 (**2**) and the phenyl spacer found in the aryl APH analogues were envisioned. One such combination involved phosphonoalkyl-substituted 1-carboxytetrahydroisoquinolines, where the alkylphosphonate side chain

Table VII. Results of Cambridge Structural Database[23] Search

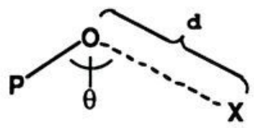

refcode	d	θ	refcode	d	θ
ACETPA	2.63	120	HISAPH	2.69	126
ADPOSM	2.86	104		2.73	124
AFCYDP	2.75	127	IMDAZP	2.71	118
AGUAHP	3.09	115	IPRAZP	2.66	117
	2.90	114	LARGPH	2.84	125
AMAFAP	2.79	114	MGUANP	3.04	120
	2.77	116	MINOSP	2.90	108
AMPETP	2.80	119	PUTRDP	2.79	113
AZURPH	2.84	126	RBADPM	2.76	127
BALVAL	2.73	124		2.71	138
BORTAD	2.61	117		2.66	129
	2.61	104	THPPTH	2.73	138
CILHUA	2.41	124		2.83	120
CRBAMP	2.42	130		2.47	151
	2.98	107		2.46	119
DAZYAE	2.61	126		2.53	164
DOFJOX	2.70	120	TLPTUR	2.94	139
	3.30	126	URECAP	2.61	115
DUJPED	2.53	117		2.68	111
	2.51	117	DOPSUW	2.82	116
EPHDHP	2.81	135		2.56	140
ETHDPH	2.45	119	DUNHID	3.04	125
GLYCPH	2.59	112		2.94	108
GLYGLP	2.50	125			
HCCOXE	2.59	118	mean	2.73	122
	2.96	132	std dev	0.19	11
			N	49	49

Table VIII. Summary of Results of Brookhaven Protein Databank[24] Search[a]

		number of interactions			
refcode	resolution, Å	side chain	backbone	water	total
1FX1	2.0	4	5	0	9
1GPD	2.9	0	2	0	2
1HHO[b]	2.1	1	0	0	1
2GRS	2.0	4	3	0	7
2MDH	2.5	2	5	0	7
2SNS	1.5	3	0	0	3
2TGD[b]	2.1	0	0	2	0
3DFR[b]	1.7	7	7	6	20
3FXN	1.9	4	5	0	9
3LDH	3.0	3	4	0	8
3PTP[b]	1.5	2	3	0	5
4FXN	1.8	5	7	0	12
5ADH[b]	2.9	1	1	3	5
5LDH	2.7	3	1	0	4
5RSA[b]	2.0	2	1	1	4
6ADH	2.9	4	6	0	10
7CAT[b]	2.5	2	1	1	4
8CAT[b]	2.5	3	2	0	5
			grand total		122

[a] A listing of individual observations and a statistical (frequency) analysis of the data can be found in the supplementary material. [b] X-ray contains solvent (H_2O) molecules.

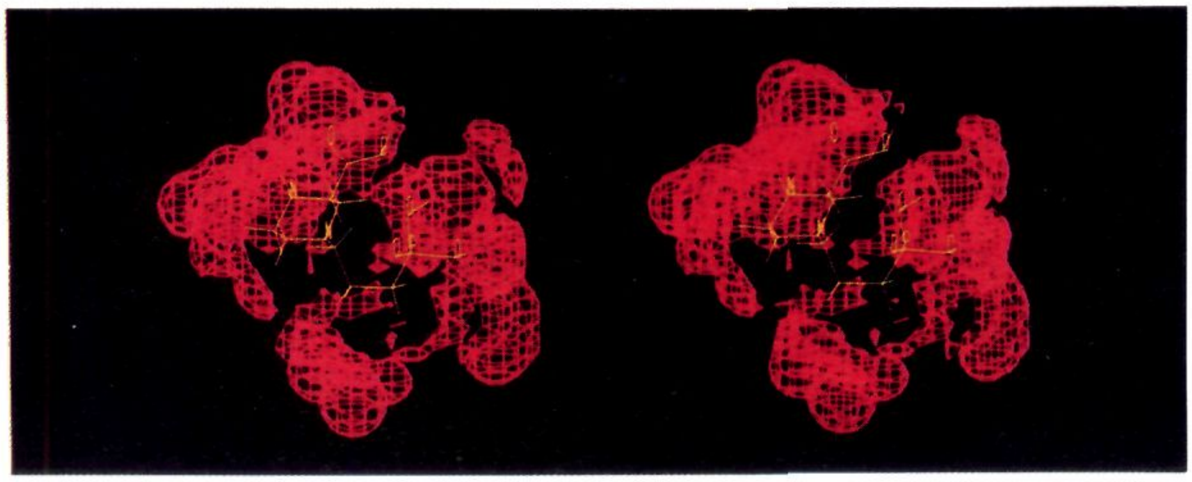

Figure 16. Stereoviews of the entire severe excluded volume, with the fit version of **1** included for reference.

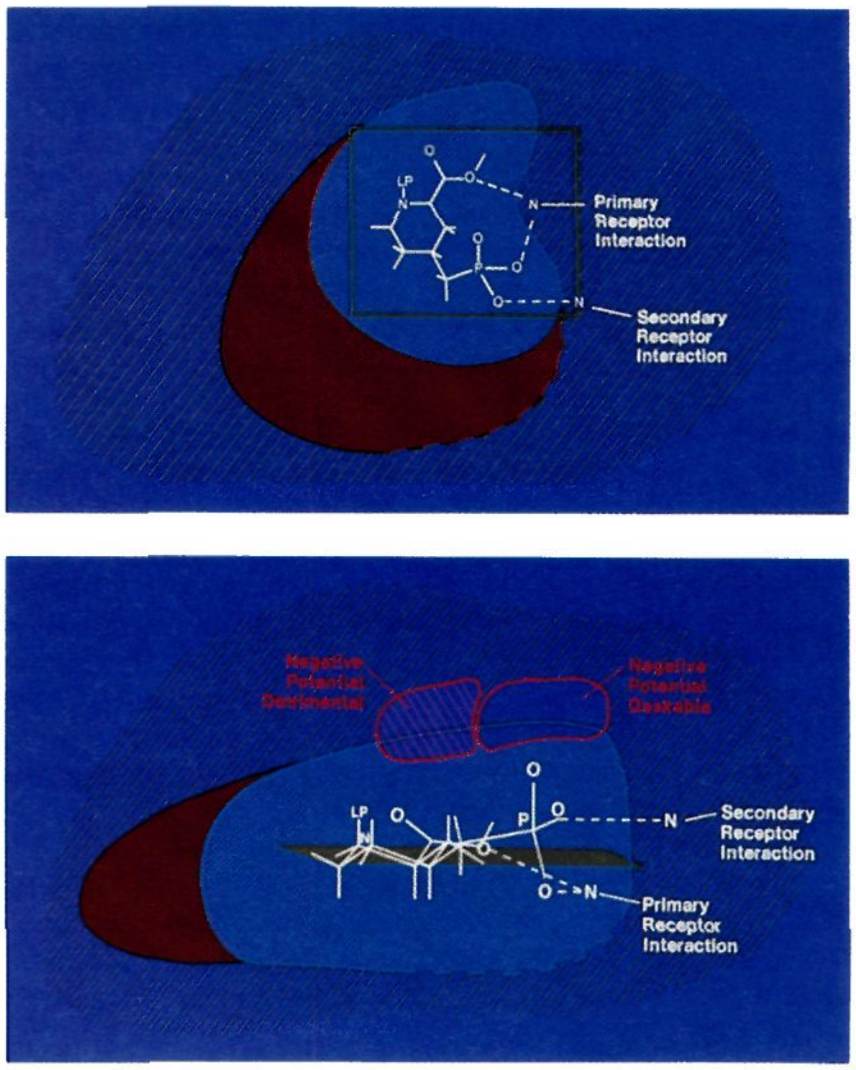

Figure 17. Summary of the NMDA competitive antagonist pharmacophore model, from two views (top-down and edge-on to the piperidine ring of **2**). The plane defined by the piperidine ring is shown in light green, and the receptor (active) volume appears in light blue (Table III, Figure 13).

has four possible sites of attachment on the aromatic ring. These analogues were selected initially on the basis of their synthetic accessibility. However, at this preliminary stage, prediction of optimum substitution patterns was difficult.

As the antagonist pharmacophore model developed, it became apparent that fusing an aromatic ring onto the 4 and 5 positions of the piperidine ring of **2** was sterically tolerated and would result in a relatively rigid, lipophilic[32] 3-carboxytetrahydroisoquinoline ring system. Addition of phosphonoalkyl side chains at the appropriate ring position would then result in analogues capable of interacting directly with the two receptor interaction points in the appropriate hydrogen-bonding geometry, while remaining within the confines of the active-volume region. On the basis of the antagonist pharmacophore model, low energy conformations of the 5-substituted analogues were predicted to fulfill these criteria. Furthermore, knowledge of electronic requirements at the receptor suggested that the periodicity in affinity observed in the AP4-5-6-7 and **82**–**83**–**1**–**84** series (Table VI) would be mimicked by the alkyl homologues, **87**–**88**–**89**.

The synthesis and a detailed discussion of the SAR of both the 1- and 3-carboxytetrahydroisoquinolines is described below. Figure 19 depicts the fit of one of the more potent analogues (**89**) in the competitive antagonist pharmacophore model.

Chemistry

In general, directly bonded aromatic phosphonic acids were prepared by palladium(0)-mediated coupling reactions of aromatic bromides or triflates with diethyl phosphite.[33] In cases where a 2-phosphonoethyl fragment was desired, it was possible to utilize a palladium(II)-catalyzed coupling of an aromatic bromide or triflate with diethyl vinylphosphonate followed by hydrogenation of the double bond.[34] Incorporation of phosphonomethyl substituents was accomplished by displacement of an appropriately substituted benzyl bromide with sodium diethyl phosphite.

Initially, 1-carboxy-5- and 7-(phosphonoalkyl)tetrahydroisoquinolines were prepared by the route shown in Scheme I. Introduction of 5-phosphono or 5-phosphonoethyl substitution was accomplished by palladium catalysis of either bromo- or trifluoromethanesulfonyl-substituted isoquinolines. Introduction of the 1-carboxylic acid was effected by modified Reissert–Henze chemistry.[35] N-Oxidation of the isoquinoline with *m*-chloroperoxybenzoic acid followed by heating with trimethylsilyl cyanide and triethylamine afforded the nitrile, which was subsequently converted to an amide by heating in concentrated sulfuric acid at 90 °C. The amide intermediates were hydrogenated and then further hydrolyzed in refluxing aqueous 6 N HCl for 24–48 h to provide the target compounds.

A second method utilized for the preparation of phosphono- and phosphonoalkyl-substituted 1-carboxytetrahydroisoquinolines is illustrated in Scheme II. In this case, the intramolecular amidoalkylation reaction of ethyl [2- or 4-(bromophenyl)ethyl]carbamates (**123** and **124**) with glyoxylic acid provided the appropriately substituted 1-carboxytetrahydroisoquinolines.[36] A rather unexpected finding was the ease with which the ring brominated and presumably moderately deactivated phenethylamines cyclized,[37] since facile cyclization of an electron-deficient ring is unusual. Elaboration of the 7-bromoisoquinoline **126** to the phosphono and phosphonoethyl derivatives **96** and **98** proceeded smoothly. However, in the case of 5-bromotetrahydroisoquinoline **127**, palladium(0)-catalyzed phosphonate replacement proceeded sluggishly, requiring extended reaction times and affording the coupled material **129** in poor yield. In addition, purification of the reaction mixture was complicated by the presence of triphenylphosphine oxide, which could not be completely removed from the product by chromatography. This mixture could, however, be hydrolyzed and the triphenylphosphine oxide removed by extraction with ether.

Extension of this amidoalkylation reaction to phosphonomethyl-substituted (2-phenylethyl)carbamates **139** and **140** provided entry into the 6- and 7-(phosphonomethyl)tetrahydroisoquinoline derivatives **95** and **97** (Scheme III). Although the amidoalkylation reaction of **139** with glyoxylic acid gave a 6:1 ratio of regioisomeric products **141** and **143**,[38] Fischer esterification of this

---

(32) The isoquinoline **89** has a calculated log *P* (using version 3.54 of the CLOGP program from Daylight, Inc. of Pomona, CA) 1.4 log units higher than that of **1** (the contribution from the PO_3H_2 moiety was excluded from both calculations).

(33) Hirao, T.; Masunaga, T.; Oshiro, Y.; Agawa, T. A Novel Synthesis of Dialkyl Arenephosphonates. *Synthesis* **1981**, 56–71.

(34) Chen, Q.; Yang, Z. Palladium-catalyzed Reaction of Phenyl Fluoroalkanesulfonates with Alkynes and Alkenes. *Tetrahedron Lett.* **1986**, 1171–1174.

(35) Vorbruggen, H.; Krolikiewicz, K. Trimethylsilanol as Leaving Group; III[1]. A Simple One-Step Conversion of Aromatic Heterocyclic *N*-oxides to α-Cyano Aromatic *N*-Heterocycles. *Synthesis* **1983**, 316–319.

(36) Ben-Ishai, D.; Satay, I.; Peled, N.; Goldshare, R. Intra vs Intermolecular Amidoalkylation of Aromatics. *Tetrahedron* **1987**, 439–450.

(37) Grazi, C. O.; Corral, R. H.; Giaccio, H. Synthesis of Fused Heterocycles: 1,2,3,4-Tetrahydroisoquinolines and Ring Homologues via Sulphonamidomethylation. *J. Chem. Soc., Perkin Trans. 1* **1986**, 1977–1982.

(38) The regioisomer ratios were determined by integration of the ^1H NMR spectra.

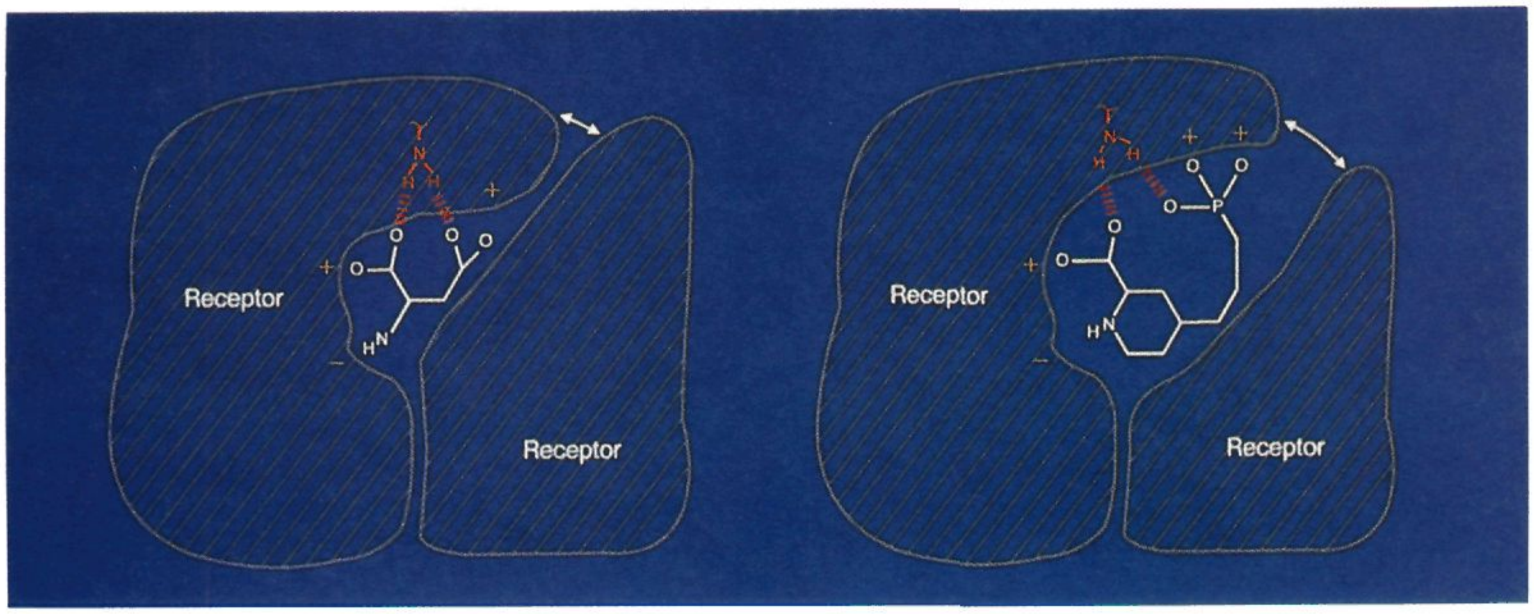

Figure 18. Hypothetical NMDA agonist (left, with L-ASP (**5**) bound) and antagonist (right, with CPP (**1**) bound) receptor sites. It is proposed that agonists and antagonists bind to the same receptor site off of one face (west and northwest), interacting with the same receptor moieties (a hypothetical receptor amine has been added as an illustration), but the larger antagonists bind to additional sites to the north and prevent a conformational change in the receptor that is responsible for agonist activity.

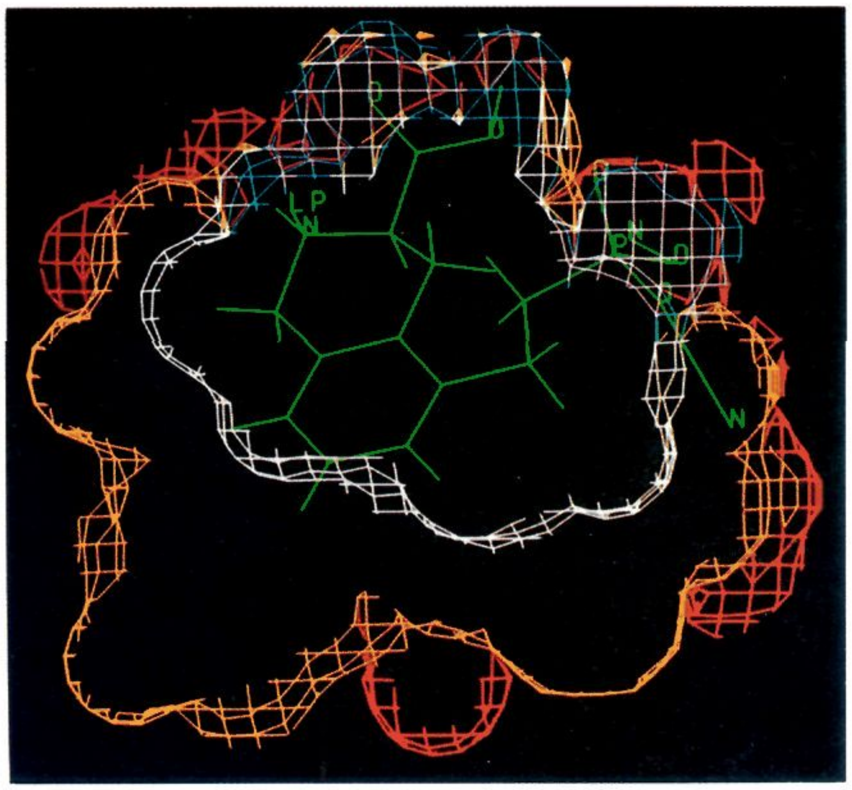

Figure 19. Fit of the designed isoquinoline **89** in the pharmacophore model. Surfaces correspond to receptor tolerated and excluded volumes; see Figure 15.

mixture unexpectedly provided **144** in greater than 95% isomeric purity,[38,39] perhaps due to a neighboring group interaction between the carboxylate and phosphonate functionalities in **143**.

Efforts toward the preparation of (phosphonoalkyl)-3-carboxytetrahydroisoquinolines also relied on amidoalkylation technology. Initial attempts to effect the cyclization of *N*-acetyl-4-bromophenylalanine (**147**) with formaldehyde failed (eq 1); subsequent replacement of the

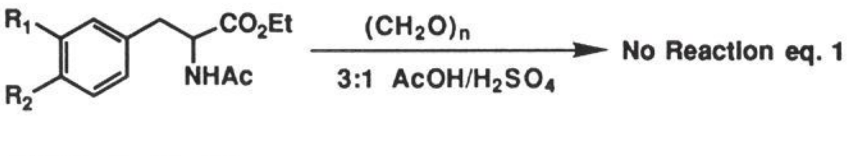

147 $R_1=H$, $R_2=Br$
148 $R_1=CH_2PO_3Et_2$, $R_2=H$

p-bromo substituent with a *m*-phosphonomethyl group (**148**) failed as well. However, transformation of the acetamidomalonate derivatives **149** and **150** to the carbamoyl esters **154** and **156**, followed by treatment with formaldehyde, provided the required methyl 5- and 7-bromotetrahydroisoquinoline-3-carboxylate intermediates **157** and **158** in moderate yield (Scheme IV). Elaboration to the target compounds **87**, **89**, **91**, and **93** was accomplished using standard conditions. Subsequently, it was discovered that modification of the acetamidomalonate adducts was not necessary, since the corresponding diethyl *N*-(ethoxycarbonyl)malonates **169**–**172** also underwent facile amidocyclization to afford the target tetrahydroisoquinolines directly (Scheme V). As in previous examples, it proved possible to simultaneously deprotect and decarboxylate these compounds in refluxing 6 N HCl. In addition to the phosphonomethyl derivatives **88**, **90**, and **92**, the propanoic acid derivative **99** was also prepared utilizing a palladium(II) coupling of the 5-bromo derivative **173** with ethyl acrylate, followed by hydrogenation and hydrolysis.

Structure–Activity Relationships

The [^{3}H]CPP receptor binding affinities for the entire set of 1- and 3-carboxytetrahydroisoquinolines, together with quinoline **21**, are shown in Table IX. As mentioned above, an initial set of these compounds was prepared to investigate the effect of further constraining the conformational flexibility of a previously reported[11] series of phenyl-spaced phosphonoalkanoic acids while retaining the aryl moiety to maintain increased lipophilicity relative to the alicyclic antagonists AP5 (**3**) and AP7 (**4**). Therefore, it is interesting to compare the SARs of the two series, in light of the antagonist pharmacophore model described above.

For the 1-carboxyisoquinolines **96**–**98**, which correspond to the meta,0,*x*-substituted phosphonoalkylphenylglycines, roughly comparable receptor binding was observed (Table IX). Of interest are the affinities of **94** and **96**, which represent locked syn and anti forms of the meta,0,0 analogue. Consistent with the pharmacophore model, a syn orientation of the two acidic functionalities is preferred. The reduced potency of **95** over the para,0,1 analogue can be explained by excluded volume occupation in reaching the primary receptor point and the fact that the secondary receptor point could not be adequately reached due to steric clashes with the phenyl ring. This is because the phenyl ring in the para,0,1 analogue could be rotated approximately 90° out of the plane of the amino acid portion to accommodate a folding of the side chain back to the

---

(39) The regiochemistry of the major product was established by a DNOE experiment.